Noname manuscript No.
(will be inserted by the editor)

Characteristics of the pulsating jet flow through a dynamic glottal model with a lens-like constriction

Willy Mattheus · Christoph Brücker

Received: date / Accepted: date

Abstract A computational study of the pulsating jet in a squared channel with a dynamic glottal-shaped constriction is presented. It follows the model experiments of Triep and Brücker (2010) with the cam-driven model that replicates the dynamic glottal motion in the process of human phonation. The boundary conditions are mapped from the model experiment onto the computational model and the three dimensional time resolved velocity and pressure fields are numerically calculated. This study aims to provide more details of flow separation and pressure distribution in the glottal gap and in the supraglottal flow field. Within the glottal gap a "vena contracta" effect is generated in the mid-sagittal plane. The flow separation in the mid-coronal plane is therefore delayed to larger diffuser angles which leads to an "axis switching" effect from mid-sagittal to mid-coronal plane. The location of flow separation in mid-sagittal cross section moves up- and downwards along the vocal folds surface in streamwise direction. The generated jet shear layer forms a chain of coherent vortex structures within each glottal cycle. These vortices cause characteristic velocity and pressure fluctuations in the supraglottal region, that are in the range of 10 to 30 times of the fundamental frequency.

Keywords g
lottal jet ; axis-switching ; numerical simulation ; experimental validation ; phonation

W. Mattheus
Department of Otorhinolaryngology, Division of Phoniatrics and Audiology, Faculty of Medicine "Carl Gustav Carus", Technische Universität Dresden, Dresden, Germany E-mail: willy.mattheus@uniklinikum-dresden.de

Ch. Brücker
City University London, Dept. Mechanical Engineering and Aeronautics, Northampton Square, London, UK E-mail: christop.bruecker@city.ac.uk

1 Introduction

The process of human phonation is characterized by a pulsating jet flow including fluid-structure-interaction with the vocal folds. Brief puffs of air driven by a transglottal pressure difference are transmitted periodically from the vibrating glottal gap into the vocal tract. The flow modulation by the vibratory motion of the vocal folds surface leads to compression and rarefaction waves within the glottal source region that are propagating to the lungs and throughout the upper vocal tract that acts as a filter by which formants are produced for vocalization.

The main sound source is generated by the pulsating jet flow. It causes a dipole sound source that is induced by the net force exerted by the vocal folds surface on the fluid in streamwise direction [1]. Vortex-induced sound, which is of quadrupole character, usually plays a minor role in healthy phonation because this quadrupole source is expected to be at least one order of magnitude, i.e. 20dB, lower than the dipole source. Nevertheless, the quadrupole source is always inherent in the process of phonation and even becomes essential when one is using voiceless sounds, e.g. in whispering [2], or when it comes to the question of voice quality. Past studies by [3,2,4,1,5] and recent studies by [6,7,8] reveal the importance of considering also the quadrupole sound source type. A review about the progress of fluid dynamic and aeroacoustic computation of voice generation is given by [9,10,11].

Numerical simulations of the unsteady glottal flow may help to clarify the different nature of sound sources in the glottal area, while experiments are difficult to conduct in this region. However, most of the aeroacoustic simulations are based on a 2D representation of the flow and acoustic fields, due to the computational costs

by higher order numerical schemes. On the other hand, the 3D effects of glottal contours and motion may yield a different flow structure in a space and time, and as a consequence also a different acoustic source distribution. This has been demonstrated by comparing the results of 3D flow simulations for a 2D rectangular and a 3D lens-like type of glottal constriction, see [12]. It has been further shown that 2D simulations of glottal flow in principle are unable to describe the vortex dynamics in a realistic way because the underlaying 2D equations exclude any effect of vortex stretching and tilting.

Further simulations of the three dimensional flow field in the laryngeal region were carried out by [13] including the ventricular folds. They obtained the pressure distribution along the vocal fold surfaces and could show the effect of the false vocal folds on the pressure distribution. [14] investigated a hemilarynx configuration of a static divergent glottal model. The flow rate was kept constant and they observed intraglottal vortex shedding at non-dimensional frequencies of St=0.013 and 0.022 and vortex shedding frequencies further downstream of St=0.143 (frequency ratio of 10). [15] investigated the supraglottal jet flow concerning the possible existence of the so-called Coanda effect. They found no clear Coanda effect which agrees with our results in the comprehensive study of [12] when the glottal channel is modeled as a 3D-flow. Further investigations by [16] showed the three dimensional character of the glottal jet in a fully coupled fluid-structure interaction model and demonstrate good qualitative similarity of spatio-temporal structures to the model of [17] and [12].

However, no quantitative data of numerical studies with the cam-model has been shown yet, since the focus of the study by [12] was on demonstrating the differences of 2D and 3D simulations of the transglottal flow. The present paper aims to fill this gap and contributes to a further understanding of the 3D jet formation and temporal evolution of pressure distribution in the glottal gap in the dynamic cam-model. Section 2 describes the used numerical version of the cam-model and the dynamic boundary conditions applied to it. The pulsating flow-rate through the lens-like contoured constriction corresponds to the flow conditions described in the model experiments by [18,17]. Results of the computed flow fields compared to the model experiments are presented in section 3. 3D flow visualizations, velocity profiles, a transglottal pressure waveform, the location of flow separation within the glottal gap, supraglottal hydrodynamic pressure fields and their frequency content are presented.

2 Computational Model

2.1 Geometry

The geometry of the numerical model of the glottal constriction is based on the physical model presented by [17] and [19], henceforth referred to as "cam-driven" model. As depicted in figure 1, the model vocal folds are placed in a horizontal section of an U-shaped water filled duct with a water column at both ends by which a pressure head is imposed. The model vocal folds are rotating membrane covered cams. Their rotation periodically opens the glottal gap and thus generates the pulsating jet flow. They perform a time-varying prescribed movement that leads to a lens-like opening in the transversal cross-section and a convergent to divergent nozzle shaped constriction in the coronal cross section. Figures 2,3 and 4 depict the temporal pattern of the convergent to divergent change and in coronal cross-section and the lens-shaped contour in transversal cross section,respectively. This configuration was mapped from the model experiment onto the computational domain, so that the spatio-temporal behavior of the glottal constriction matches. The approach of a cam-driven model was chosen because it ensures a reproducible behavior of the supraglottal flow field that is focused on in this study. The supraglottal flow field periodically develops under defined boundary conditions.

The dimensions of the glottal model are given in figure 2 based on the width D of the channel which is related to the diameter of the human trachea with $D \approx 0.02m$. The glottal gap with its lens-shaped transversal cross-section has a much smaller area than the trachea. It's reduced by a factor of about 18. In the coronal cross-section, the constriction is contoured like a nozzle with a smooth convergent entry and a divergent exit.

2.2 CFD model

The pressure driven pulsating air flow through the oscillating glottal constriction is characterized by the following fluid dynamic dimensionless quantities:

- Mach-number $Ma = u/a$
- Reynolds number $Re = (u_{glottis} \cdot d)/\nu$
- Strouhal number $Sr = (f_0 d)/u_{glottis}$
- Euler number $Eu = \Delta p / \left(\rho u_{glottis}^2\right)$

The characteristic parameters are the glottal gap width d, the velocity $u_{glottis}$ in the glottal gap, the fundamental frequency f_0 of the pulsating jet flow through the glottal gap, the driving trans-glottal pressure head Δp as depicted in figure 1, the density ρ and the viscosity ν

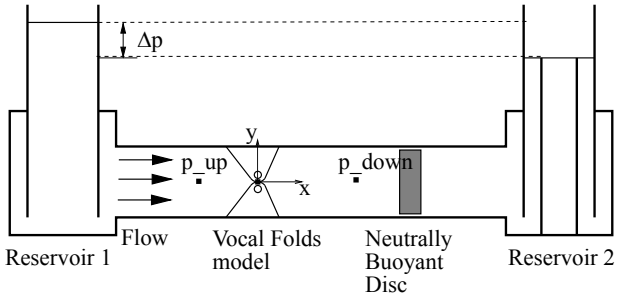

Fig. 1 Sketch of the experimental setup that was used for the measurements of flowrate and pressure difference, the setup is used by [20] and [17] wherein the flow is driven by a pressure difference Δp of two connected water columns, the flowrate was measured by the displacement of a neutrally buoyant disc and the transglottal pressure difference is measured by pressure sensors located at p_{up} and p_{down}

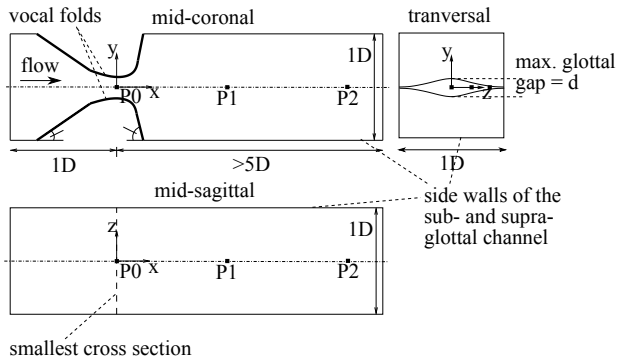

Fig. 2 Geometrical shape of the computational domain with dimensions based on the channel width D (derived from the tracheal diameter of about 0.02m), the glottal cross section is depicted in fully opened configuration with the maximum glottal gap d, P0 to P2 are defined for the evaluation of flow quantities

of air. The maximum value of the velocity $u_{glottis}$ in the glottal gap is given by [21] with approximately 30 m/s. The Mach number arising from this intra-glottal velocity is $Ma \approx 0.1$. Therefore the computed flow fields in the numerical simulation are considered to be incompressible. This approximation is approved by other authors, e.g. [22,23,24]. All data of the physiological transglottal airflow during phonation and the appropriate values of the fluid dynamic dimensionless quantities are summarized in table 1 and satisfied by the "cam-model" too.

The numerical computation works independently of this scaling because the governing equations employed in the computational model dimensioned by Strouhal, Reynolds and Euler Number so that the physical medium is not relevant as long as the fluid dynamic laws of similarity are conserved.

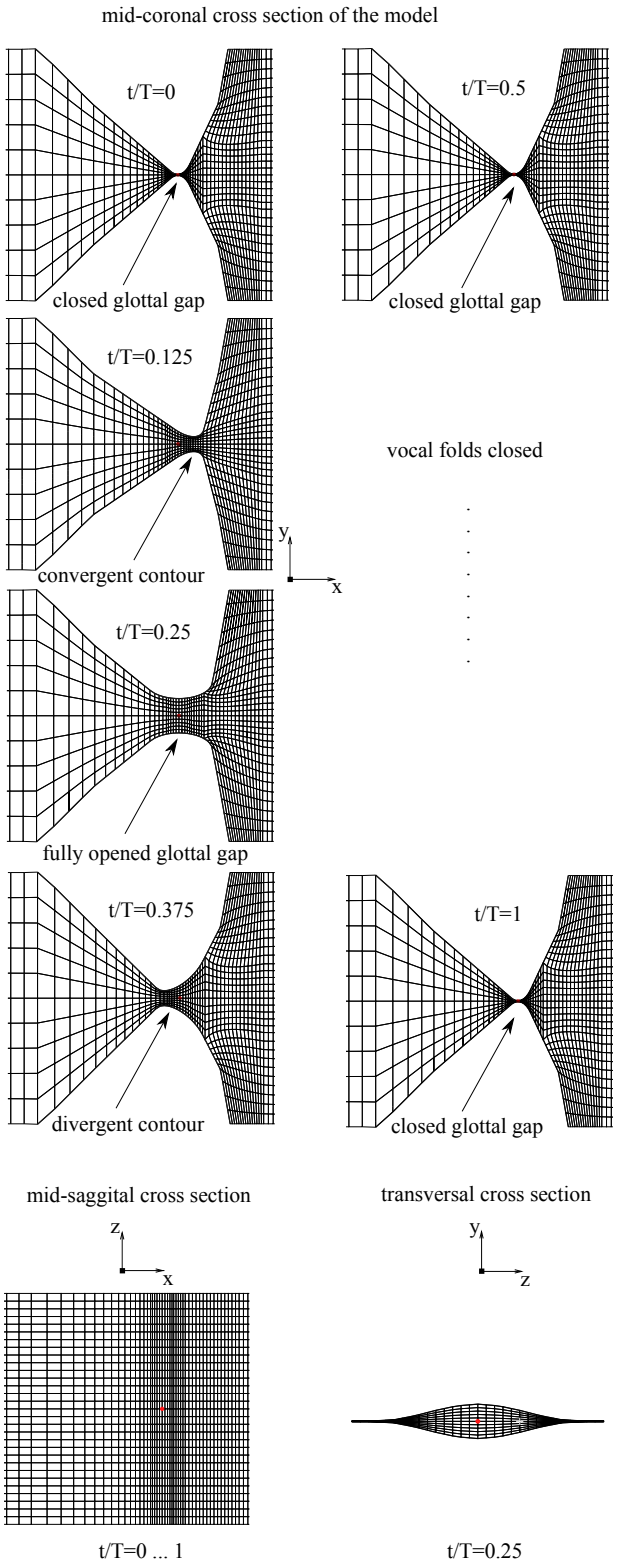

Fig. 3 Finite Volume Mesh of the computational domain in mid-coronal, mid-sagittal and transversal cross section, the element size is based on the channel width D, the edge length (EL) equals 1/10th of D at the inlet boundary and is reduced in the inner glottal and supraglottal region to values of 1/60th of D, no movement of mesh points in the mid-sagittal plane due to symmetry

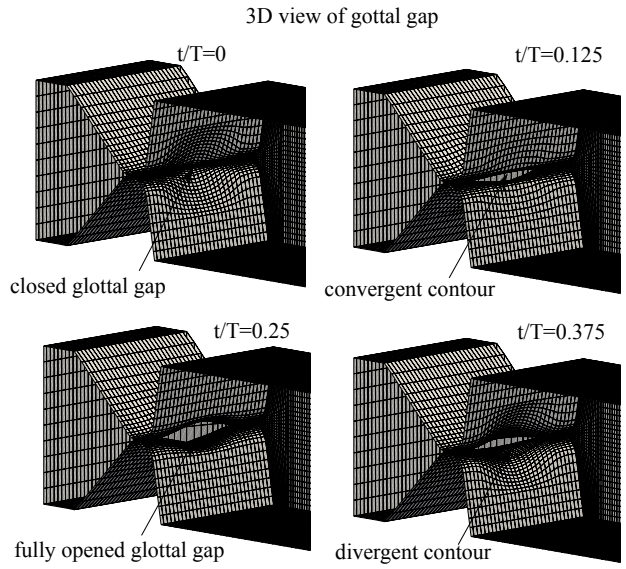

Fig. 4 Finite Volume Mesh of the computational domain in a 3D view through the side wall onto the dynamic glottal gap for 4 successive time-steps of the glottal motion cycle, the open quotient (OQ) is 0.5 and the inverse fundamental frequency T

Table 1 Values of the transglottal air flow ([21]) and the corresponding dimensionless quantitiy satisfied by the "cam-model" by [18]

dimensions	
tracheal diameter D	20 mm
max. glottal gap width d	2.7 mm
physical properties	
density ρ	$1.2 kg/m^3$
kinematic viscosity ν	$1.5 \cdot 10^{-5} m^2/s$
dynamic viscosity η	$18 \cdot 10^{-6} kg/ms$
similitude theory	
intraglottal velocity $u_{glottis}$	25...35m/s $\approx$ 30m/s
fundamental frequency f_0	135 Hz
pressure head Δp	600Pa
Mach number	$Ma = u/a \leq 0.1$
not conserved by the model, assumption of incompressible flow	
Reynolds number	$Re = (u_{glottis} \cdot d) / \nu = 5400$
conserved by the model	
Strouhal number	$Sr = (f_0 d) / u_{glottis} = 0.012$
conserved by the model	
Euler number	$Eu = \Delta p / \left(\rho u_{glottis}^2\right) \leq 1$
conserved by the model	

The CFD model is based on the time-dependent, incompressible Navier-Stokes equations for Newtonian fluids that read

$$\nabla \cdot \mathbf{u} = 0 \tag{1}$$

$$\frac{\partial \mathbf{u}}{\partial t} + \mathbf{u} \cdot \nabla \mathbf{u} = -\frac{1}{\rho} \nabla p + \nu \nabla^2 \mathbf{u} \,. \tag{2}$$

Equations (1) and (2) are numerically solved with the finite-volume method in a cell-centered formulation on a fully block-structured grid with the open-source CFD code OpenFOAM published by [25].

For the interpolation of the convective flux terms a Total-Variation-Diminishing (TVD) scheme with a flux limiter function $\psi(r) = max\left[0, min\left(2 \cdot r, 1\right)\right]$ [26] is employed. The smoothness parameter r is defined by the ratio of successive gradients. A central differencing scheme with non-orthogonal correction is used for the discretization of the diffusive fluxes. Time integration of equations (1) and (2) is performed with a scheme which blends Crank-Nicholson and Euler implicit scheme by a weighting factor of 0.8 and 0.2, respectively. The time step is kept constant with $\Delta t/T = 2 \cdot 10^{-5}$ in all simulations. Mass conservation is enforced with the transient PISO algorithm [27] with a collocated arrangement of pressure and velocity. The formulation of the algorithm is in line with the correction of [28] in order to avoid non-physical oscillations in the flow variables. The pressure equation is solved with an algebraic multi-grid solver with Gauss-Seidel smoothing. The momentum equations are solved with the bi-conjugate gradient algorithm of [29], where incomplete LU decomposition is used for preconditioning the system. The residual errors per time step are of the order 10^{-8} for the momentum equation and for the pressure equation.

This formulation of the CFD model has been validated in a recent study of starting jet flow by [30] for a static model of glottal gap using the same geometry as herein. A validation of the dynamic glottal model used in this study is given in the results section 3 of this paper.

The computational domain consists of moving boundaries which generate a time-varying glottal gap with the maximum opening area $A_{max} \approx 20 mm^2$ and a normalized waveform as depicted in figure 5. The mesh points of the boundaries faces are displaced during computation so that the time-varying shape of the constriction is reproduced. The equation for the displacement of the inner grid points of the computational mesh is then calculated by the following equation

$$\nabla \cdot (D_{\text{diff}} \nabla \Delta_P) = 0 \tag{3}$$

where D is the Diffusion Coefficient and δ the displacement of the mesh point P. Then the calculation is continued on the updated mesh where the initial values are interpolated from the previous mesh.

2.3 Boundary conditions

The pulsating flow is generated by applying the periodic waveform function depicted in figure 5 as a time-varying uniformly distributed velocity value $u^{in}(t)$ (plug flow) onto the inflow boundary of the computational domain. Synchronous to this, the motion of the vocal fold surfaces that leads to the opening area function depicted in figure 5 is prescribed to the numerical model by the displacement of the boundary points of the left and the right model vocal fold.

The waveform of the flowrate is taken from the measurements with the model of [17]. Its configuration and the method of flow-rate measurement with the neutrally buoyant disc are depicted in figure 1. The pressure head Δp between reservoir 1 and 2 is set to $\Delta p = 600Pa$ and represents a lower value in the process of human phonation. The normalized waveform reproduces the one documented by [31] that was obtained by the method of inverse filtering. Some characteristics of the waveform are also captured: zero flow rate for half of the cycle time so that an open quotient of 0.5 is realized, a temporarily slightly delayed maximum of the flow rate compared to the opening area, and a 6dB decline in the first 5 harmonics of the frequency spectrum, which is a typical value for glottal source spectra as stated by [32] and proven by [33].

The no-slip condition $\mathbf{u}_{wall} = 0$ for velocity and zero gradient condition $\partial p/\partial x_n = 0$ for pressure are defined in normal direction to each wall boundary. The pressure field values of the entire domain are given with respect to a reference value of $p_{ref} = 10^5\,Pa$ located at the outlet boundary. At initial simulation time $t = 0$ the whole flow field is at rest. In total, a number of 10 successive cycles are simulated in one simulation process, where the first cycle starts from zero velocity in the whole computational domain.

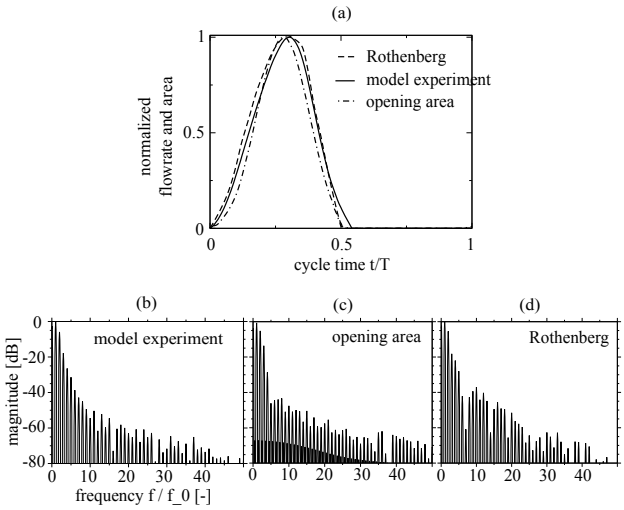

Fig. 5 Boundary condition at the inlet of the computational model: (a) Time varying area of the glottal gap, resulting volume-flow rate in the model experiment from [17], comparison to the measurements of [31], area function of the glottal gap is mapped onto the model vocal folds and the flow rate function is mapped onto the inlet boundary condition of the numerical model, (b) and (c) frequency content of the functions of subfigure (a), the spectral slope of the harmonics of the flow rate function is about -6dB/octave as suggested by various models of [32] and measurements of [33]

3 Results

Figure 6 shows the results of the numerically computed flow fields compared to the ones of the model experiment by means of flow visualization at certain instants of time within one glottal cycle. We chose a very illustrative but qualitative method to compare the global 3D flow structures and their temporal evolution. Additionally, they give a good impression of the penetration depth, the dimensions and the shape of the jet as well as the shear layer roll-up and vortex structures. The flow field is visualized by a fluorescent tracer in the model experiment and a scalar tracer field in the numerical simulation, respectively. Two main cross sections of the computational domain are depicted in the left and the right column of this figure. The x-y cross section, also called 'mid-coronal' plane, contains the minor axis of the lens-shaped orifice, that is opening and closing with a convergent and divergent shape of this orifice. The x-z cross-section, also called 'mid-sagittal' plane, contains the major axis of the lens-like orifice. Mid-coronal and mid-sagittal plane are both symmetry planes of the geometry.

A prominent effect of the flow field is the so called 'axis switching' of the glottal jet, as stated by [17]. This effect is obviously recovered by the numerical results when comparing the jet width in the different planes in figures 6. The kinematics of the imposed geometrical contours of the modeled glottis determine significantly the development of the jet. The convergent shape of the constriction during the opening phase causes a narrow jet neither spreading in mid-coronal plane nor contracting in mid-sagittal cross-section, so apparently no axis switching effect occurs in the early phase of the glottal cycle. In addition, flow downstream of the glottal walls is affected by the displacement flow generated by the glottal wall itself, too. At the state of fully opened glottis the axis switching starts to emerge and is further enhanced by the increasingly divergent shape of the nozzle and contribution by a lengthwise vena-contracta effect. The latter is observed by the convergent jet contour at the closing phase in the mid-sagittal plane.

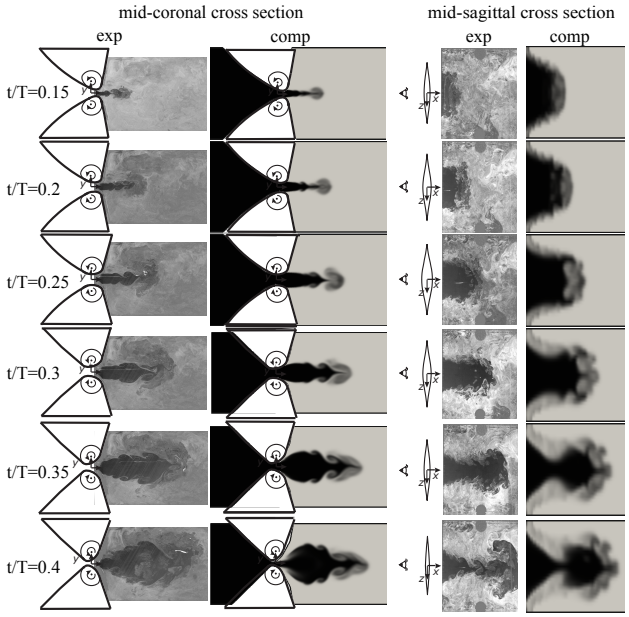

Fig. 6 Visualization of the evolution of the flow field, the results of the numerical simulation visualized by a massless tracer are compared to the results of the model experiments obtained by the method of laser induced fluorescence [17] , time instants t/T=0...1 within one glottal cycle, see figure 2 for reference

The comparison shows a good agreement of jet characteristics between experiment and CFD results. Only the very small scale structures observable in the visualization results of the model experiment are not fully resolved by the numerical simulation because of smearing of the tracer field by numerical diffusion and the limitation of the spatial mesh resolution to $\Delta x = 1/60D$. However the large coherent structures determining the main flow features, as axis-switching, shear layer roll-up and the flow separation of the jet that determines the spreading and contraction in mid-coronal and mid-sagittal plane, respectively, are well recovered by the numerical model.

Additionally, the very symmetric behavior of the flow in these planes supports the usefulness of characterization of the 3D flow structure by means of these two major planes, as stated by [17]. This symmetry is redeemed even for the n-th repeating cycle of the pulsating jet flow of the total number of n=10 cycles. Such a high degree of bi-planar symmetry is very characteristic for such a lens-like orifice as modeled herein. In contrast, symmetry is lost when a more rectangular orifice is used or even when only a 2D computation model is employed. Again, this demonstrates the importance of proper numerical model and geometrical representation of actual 3D glottal orifice contours instead of using simplified 2D geometries as discussed by [12].

As the CFD simulation runs for 10 successive cycles we are able to determine cycle-to-cycle variations of the jet position in the supra-glottal region. Figure 7 shows the ensemble-phase-averaged flow field of 10 cycles for the specified phase t/T. A systematic deflection of the jet to one side would then be visible in this representation. Since there is no deflection present, the existence of the coanda effect cannot be supported as also stated by [12,15]. Furthermore, figure 8 shows the ensemble-phase-averaged fluctuations of the velocity field. That means regions with larger cycle-to-cycle variations are indicated by higher values. The jet core shows repetitive values for every glottal cycle and follows a the center axis of the channel. No large-scale fluctuation of the jet such as flapping or attachment to one of the lateral walls is observed over the 10 cycles. Contrary the jet shear layer inherits the large fluctuations up to 20 percent of the maximum speed in the jet core. A 3D view onto the vortical flow structures is given in figure 9 by visualizing the Q-criterion of the velocity field ([34]) as an indicator for vortices. Though this region is supposed to be responsible for flow and pressure fluctuations in the frequency range higher than 10 times of the fundamental frequency f_0. This result is supported by the study of [14] and confirms our earlier observations of apparently no presence of the so-called Coanda effect in the supra-glottal region for the given model of the lens-like glottal orifice (see [12]).

Figure 10 and 11 depict the values of the transglottal pressure (difference between the points p_{up} and p_{down}) and the static pressure along a line on the surface of the left model vocal fold. The course of the static pressure along this line is plotted for certain time instants of the glottal cycle: $t/T = 0.15...0.4$. The pressure difference of the reservoirs 1 and 2 is constant during the glottal cycle and preset to $\Delta p = 600Pa$ in this model experiment. The pressure difference $p_{up} - p_{down}$ is varying throughout the glottal cycle depending on the behavior of the transglottal airflow. While the glottal gap opens the pressure difference accelerates the airflow and the difference in static pressure drops until the maximum glottal gap width is reached at $t/T = 0.25$. In the following the transglottal pressure drop increases while the shape of the glottal gap in the mid-sagittal plane changes from convergent to 'parallel' and to divergent, finally. The motion of the vocal folds leads to a rather smooth transition of the pressure distribution towards the closing state. One may speculate that this motion cycle is therefore also characteristic for relative low impact forces on the folds corresponding to a closing motion similar to a double-sided zipper as also described by [17]. This is supported by the glottal area function shown in Fig. 2 where the slope of the curve shows a

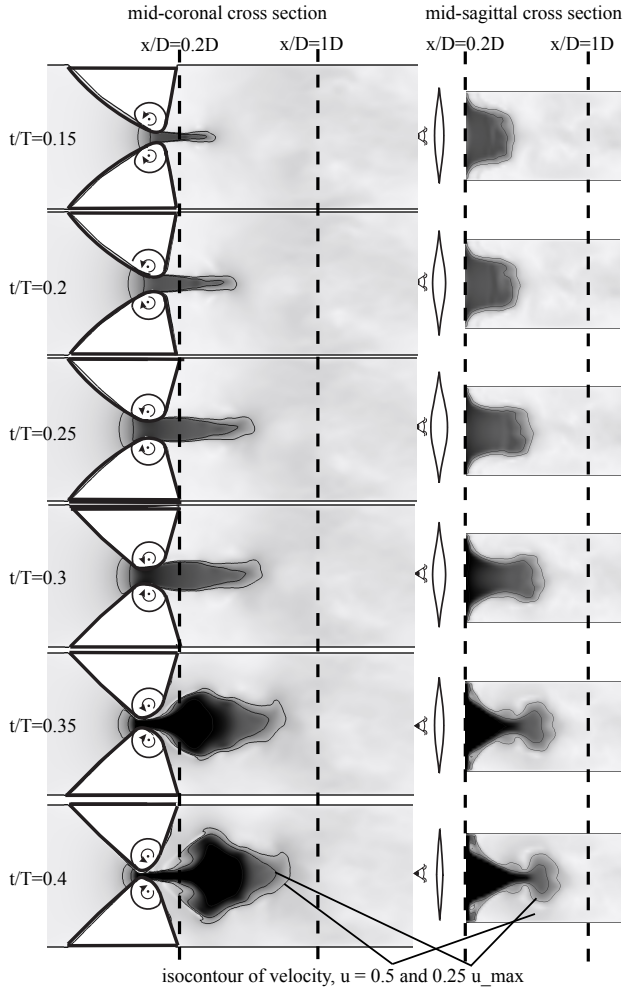

Fig. 7 Phase-locked velocity field averaged by 10 successive cycles for each displayed instant of time t/T, mid-coronal and mid-sagittal cross section are depicted and iso-contours of the velocity field are drawn, black colour indicates u_max and white equals $u = 0$

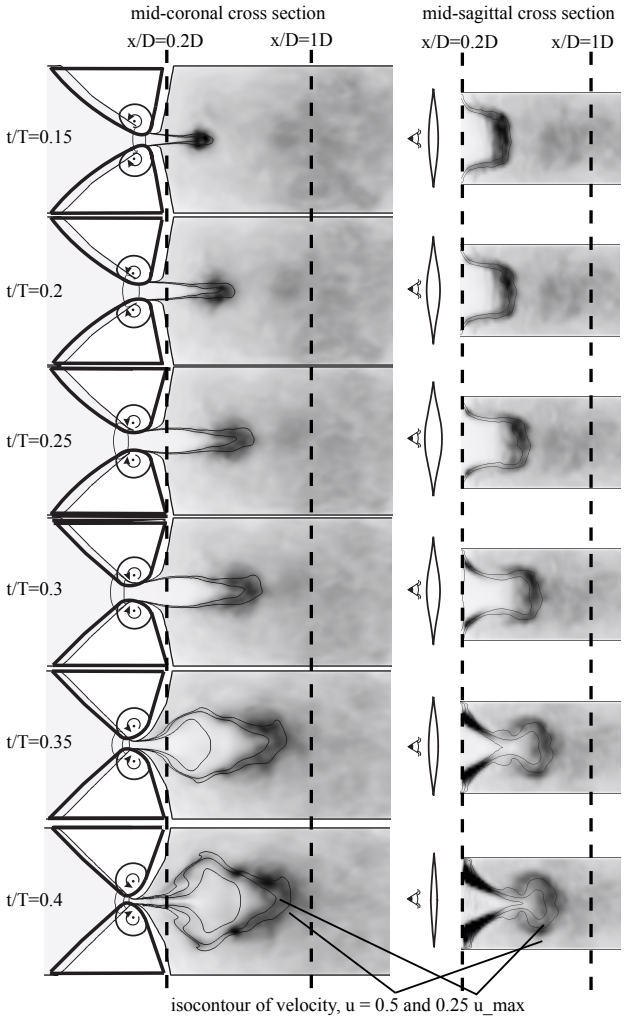

Fig. 8 Phase-locked field of the averaged cycle-to-cycle fluctuations of the velocity field, averaged by 10 successive cycles for each displayed instant of time t/T, mid-coronal and mid-sagittal cross section are depicted and iso-contours of the velocity field are drawn, black colour indicates u_max and white equals $u = 0$

continuous flattening from t/T=0.35 to full closure at t/T=0.5.

Further information on the jet dynamics is gained from the location of the separation along the glottal walls during the motion cycle. Figure 12 demonstrates the sectional streamline pattern in the mid-coronal cross section in a close-up view of the region in the glottal gap. Additionally the flow pattern in the supra-glottal region is shown by streamlines and the distribution of the static pressure field (see figure 12). The contours are color-coded with red and blue but the range of the colormap varies between the pictures of the successive time instants. This was done to enhance the contrast for visualization of the position of the pressure fluctuations. The value of the pressure is given relative to reference pressure $p_{ref} = 10^5 Pa$. The location of flow separation

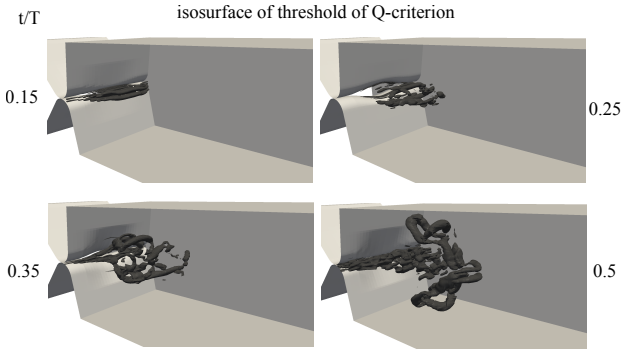

Fig. 9 3D flow structures developing during the first half of the glottal cycles $0 < t/T < 0.5$, visualized by the Q-criterion ([34]), see also [12]

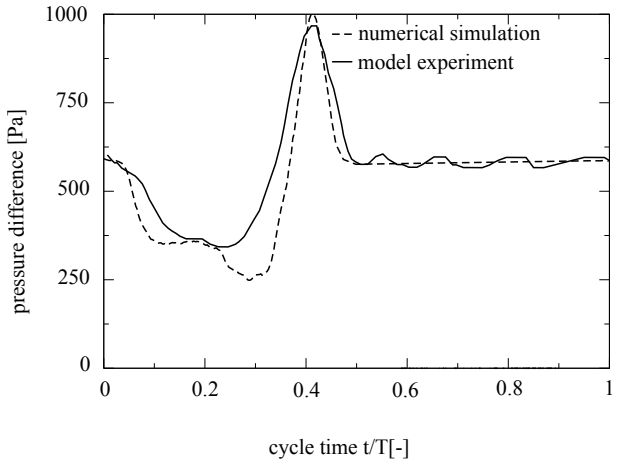

Fig. 10 Temporal evolution of the trans-glottal pressure difference between the points p_{up} and p_{down} sketched in figure 1, compared for experimental and numerical model

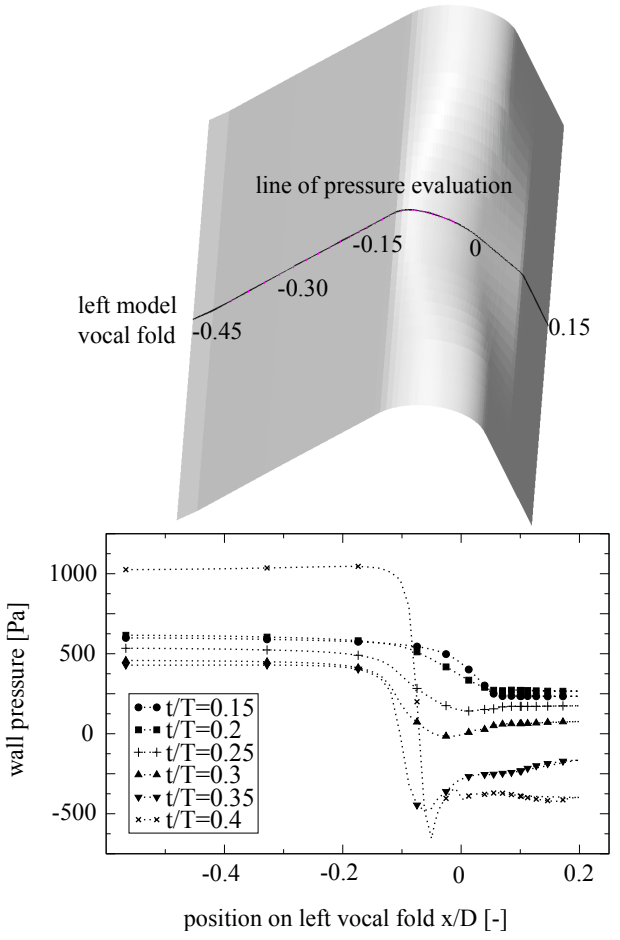

Fig. 11 Hydrodynamic pressure computed with the numerical simulation and plotted along a line in the mid-coronal plane on the surface of the left model vocal fold for successive time instants within the glottal cycle

Table 2 Location of the separation points depicted in figure 12

t/T	position x/D	mid-sagittal shape
0.05	0.037	convergent
0.10	0.058	
0.15	0.075	
0.20	0.083	
0.25	0.083	fully opened
0.3	0.050	divergent
0.35	0.000	
0.40	-0.033	
0.45	-0.017	

is indicated in the streamline pictures, computed by the condition of vanishing velocity gradient normal to the wall $\nabla u_{wall} = 0$ and summarized in table 2.

During convergent opening phase the strongest curvature of the boundary has moved to the trailing edge. The jet detaches already at the position of the smallest cross-section from the wall and remains therefore straight and compact, not divergent. When the vocal folds have passed the fully opened configuration, the location of strongest curvature moves upstream during the divergent phase of the glottal cycle and the velocity field is spread in the mid-coronal cross-section (x-y). The flow is attached to the wall up to the position $x/D = 0.1$ and finally detaches. It is obvious that flow separation in the glottal gap is delayed to lager divergence angles than the typical angle of 8 degrees known for the flow in a 2D diffuser. This also clarifies the large divergent expansion of the jet in the mid-coronal plane which is related to the 3D flow in the glottal gap.

Figure 13 shows the spanwise flow in the transversal cross-section (x-z) at position x/D=0.15. The flow is presented by the projection of the in-plane velocity vectors and areas of high and low relative pressure coded by color. The results display the generation of strong spanwise flow towards the center of the gap in the closing phase while spanwise flow is weak at the beginning of the cycle. Pressure contours demonstrate the axis-switching effect by means of re-orientation of the axis between both anti-symmetric local pressure minimum away from the mid-sagittal plane to the mid-coronal plane. Meanwhile, pressure in the center of the jet axis has reached locally a relative maximum which supports the divergent expansion of the jet. Again, these results prove the length-wise vena contracta which is generated by the lens-like shape of the glottal orifice. As seen from the pressure distribution in the mid-coronal plane in Figure 12, the low pressure regions on both lateral sides of the jet are formed like a tongue along the divergent walls (t/T=0.35). Therefore, the divergent expansion of the jet is important for the redistribution of the forces along the gottal walls in the glottal cycle.

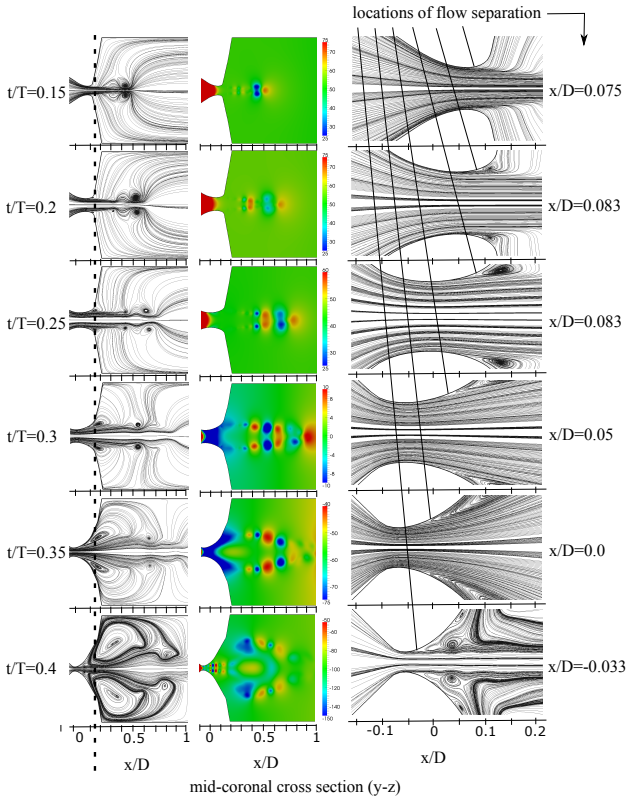

Fig. 12 left: Sectional streamlines plot in the mid-coronal cross-section showing the vortical structures generated in the jet shear layer, distribution of hydrodynamic pressure in the mid-coronal cross-section confirming the presence of a significant pressure distribution due to these vortical structures, the color range showing the hydrodynamic pressure is scaled to the minimum and maximum value occurring at each time instant, right: location of the point of flow separation the in mid-coronal cross-section, the point is indicated by separating stream lines from the boundary wall and summarized in table 2

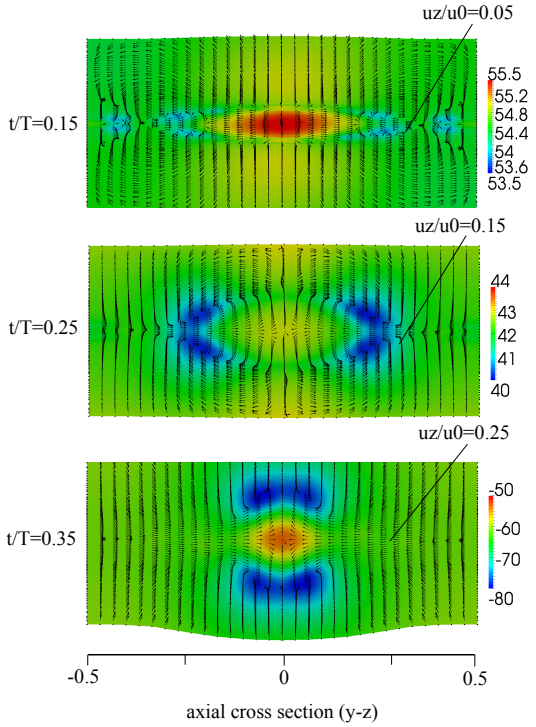

Fig. 13 Flow field in the transversal cross section (x-z) at position x/D=0.15, vector plots indicate the direction of the flow, maximum velocity u_z occurring in this plane is given relative to the jet velocity u_0, the color range showing the hydrodynamic pressure is scaled to the minimum and maximum value occurring at each time instant

Another aspect of the pressure distribution is documented by the supra-glottal pressure field in Figure 13. The locations of concentrated pressure minimum correspond to the location of vortices generated by the shear-layer roll-up. The pair-wise vortices above and below the centerline in the mid-coronal cross-sections represent the cut through a 3D vortex structure which has the shape of a deformed elliptic vortex-ring like structure. Figure 12 and 9 demonstrate that these 3D vortex structures appear as successive rows of low-pressure region over the glottal cycle. In each cycle a total number of 4 larger vortices are being shed, arranged in streamwise direction like a train of vortices. They move whith a convective velocity of approximately half the mean velocity of the jet and therefore generate a quasi-harmonic pressure variation at a fixed point in the supraglottal flow field. Figure 14(a) depicts the time course for the points P0, P1, and P2 defined in figure 2. Especially in P1 there are coherent structures observable every subsequent glottal cycle. These strutures cause the increase of the power spectrum in the range around $20 f_0$. Figure 14(b) shows the resulting frequency spectra of the velocity field at the points P0, P1 and P2 along the medial axis downstream of the glottal orifice. In the low-frequency range of $f/f0 < 12$ the spectrum decreases with approximately -7dB per octave. In the range of $12 < f/f0 < 30$, the spectrum shows a distinct rise of about 10dB above this decreasing trend which is due to the presence of the vortices in the flow field. The shedding frequency is within this range of spectral enhancement. Therefore it is concluded that the vortices contribute to flow and pressure fluctuations which might effect the acoustic spectrum of the glottal source.

4 Conclusion

A numerical model to compute the time dependent three-dimensional flow field of the low Mach number flow in a model of the laryngeal channel through the vocal folds is presented. An important feature of the simulations is the prescribed motion of the vocal folds contours during

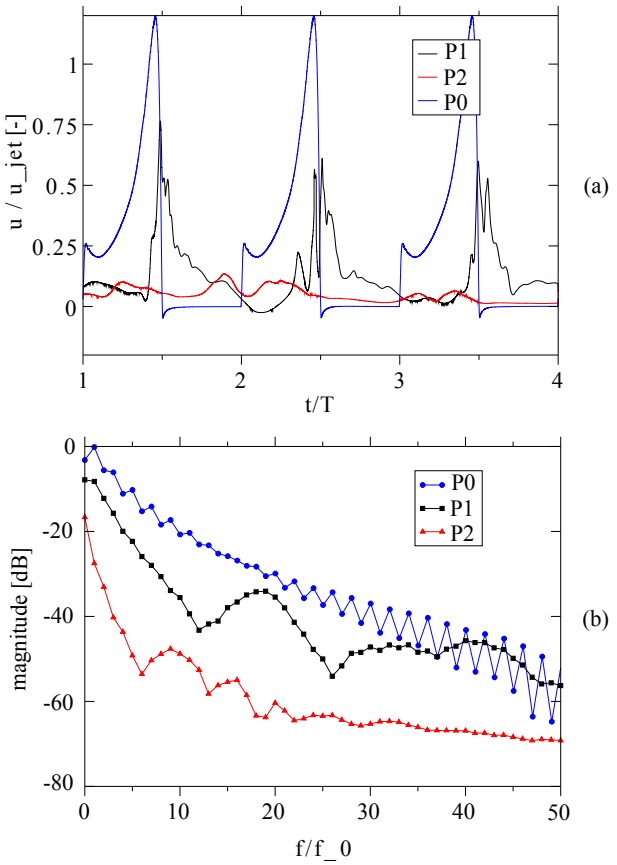

Fig. 14 (a) time course at the observation points P0, P1, P2 (see fig 2) for 3 successive glottal cycles and (b) the corresponding power spectrum of the velocity for all 10 numerically simulated glottal cycles, discrete points indicate the harmonics of the spectrum with fundamental f_0

the glottal cycle with a synchronous imprinted variation of the flow rate. Both are taken from a model experiment of [18] which allows precise and accurate validation of the numerical results. The numerical study aims at providing more detail of the flow separation process and the pressure distribution in the glottal gap, which is hard to obtain from experimental studies, especially under the condition of moving glottal walls. Comparison of the characteristic features of the jet between experiment and CFD results shows good agreement in spatio-temporal development of the jet. An illustrative way of comparison was documented herein by the method of streak-surface visualization. This rather natural and intuitive way of illustration of the flow features is generated by adding dye to the flow region upstream of the glottal gap in a mixed and homogeneous distribution. The same is done with the numerical results, where a massless tracer is continuously added on all grid cells upstream of the glottal gap and follows the fluid vector further downstream into the supra-glottal area with no slip.

The flow results show that the glottal motion in each opening- and closure cycle generates a pulsed 3D jet, which penetrates into the supra-glottal space about a distance of 1D. Within the phase of closed glottis, which is 50% of the total cycle time, the jet decays into small-scale vortices and dissipates to a degree, which does not disturb the successive cycle much. The results reveal a high degree of symmetry of the jet-flow in the supra-glottal space with respect to the mid-coronal and mid-saggital plane. Even after 10 cycles, the symmetry is of the same level. There is no sign of large-scale cycle-to-cycle variations. As a conclusion, the Coanda effect does not play a role in this type of flow with a model, which represents a 3D contour of the glottal orifice with a lens-like shape. A possible explanation of the confusion in literature is given in a former publication by our group which pinpoints the importance of glottal shape and numerical model in the interpretation of the obtained results ([12]).

Cyclic variations of the flow fields are found especially in the jet shear layer, where the generation of vortex structures induces quasi-harmonic pressure fluctuations in the range of 10-20 times the fundamental frequency, which may contribute to the acoustic spectrum of the source signal in the region of voice production. The cycle-to-cylce variations do not influence the spectral content of the pressure fluctuations much. In each cycle, a train of 4-5 vortices is generated which are convected downstream with approximately half of the local jet core velocity. The streamwise row of vortices looks relatively regular in terms of distance and convection velocity, which might be due to the interplay of temporal modulation of the jet velocity in combination with the divergent expansion of the jet. It is therefore expected that the flow and pressure fluctuations are indeed quasi-periodic and coherent within a larger area of supra-glottal space.

Flow separation from the walls of the model vocal folds determines the jet spreading and contraction in the two main cross sections of the geometry, respectively, and is responsible for the so called axis switching effect. The region of flow separation in the nozzle created in the glottal gap is moving during one glottal cycle from upstream to downstream about a distance of 0.14D. In the upstream position in the opening phase, the jet separates at the location of smallest cross-section at x/D=0.07, thus forming a rather straight jet. Later in the beginning of the closing phase, the location of smallest cross-section has moved upstream to the position x/D=-0.07. However, flow separation is largely delayed about a distance of 0.1D downstream,

thus flow separates at a position x/D=0.03. The location of separation within the diffuser appears at much larger opening angles compared to a 2D diffuser, where the literature reports a critical angle of 8. The reason for this separation delay is found in the spanwise flow in the transversal plane, which is related to a spanwise vena-contracta. At this stage of the gottal flow, strong spanwise flow is induced in the glottal gap towards the center, where maximum spanwise velocities reach 25% of the maximum axial velocity on the jet axis. Thus energy is brought into the boundary layer and flow therefore separates later in the diffuser. As a consequence, the jet experiences a strong divergent expansion in the mid-coronal plane while the jet is still converging in the mid-sagittal plane as a result of the length-wise vena-contracta.

The pressure drop across the glottal gap is varying in time with the motion cycle. Profiles of the wall pressure along the vocal fold walls of the model show that the pressure drop during the closing phase of the glottis is increasing smoothly rather than in an abrupt manner. It is already at the state of t/T=0.4 in the cycle that 90% of the total pressure head is recovered. This goes together with a rather smooth approach of the area function A(t) towards the closure of the orifice at t/T=0.5 since the slope of the curve starts decreasing early at t/T=0.35. Therefore, the pinch-off of the jet is not as abrupt as expected in a two-dimensional glottal model. This is a results of the special type of glottal closure in the lens-like constriction, where the closure process resembles a double-sided zipper which is closing from both sides in a 3D-type of motion of the contact line. From the pressure distribution it is also seen that tongue-like extensions of low pressure regions are forming at the downstream facing walls of the glottal gap. These regions originating from the complex flow of the jet and glottal motion in the late state of the cycle support the interpretation of aerodynamic pressure distribution enforcing the glottal closure in combination with a vertical upward motion of the glottal plane.

Competing interests: None declared

Ethical approval: Not required

Acknowledgement

Part of the work has been funded by the German Research Foundation (Deutsche Forschungsgemeinschaft, DFG) within the research group FOR-894 under grant no. BR 1494/13-1 which is gratefully acknowledged. Funding of the position of Professor Christoph Bruecker as the BAE SYSTEMS Sir Richard Olver Chair in Aeronautical Engineering is gratefully acknowledged herein.

References

1. W. Zhao, C. Zhang, S.H. Frankel, L. Mongeau, The Journal of the Acoustical Society of America **112**(5), 2134 (2002)
2. M. Krane, Journal of the Acoustical Society of America **118**, 410 (2005)
3. M.S. Howe, R.S. McGowan, Journal of Fluid Mechanics **592**, 367 (2007)
4. Z. Zhang, L. Mongeau, S.H. Frankel, S. Thomson, J.B. Park, Journal of the Acoustical Society of America (JASA) **116**, 1720 (2004)
5. Z. Zhang, L. Mongeau, S. Frankel, S. Thomson, J. Park, The Journal of the Acoustical Society of America **112**(3), 2147 (2002)
6. R.S. McGowan, M.S. Howe, The Journal of the Acoustical Society of America **131**(4), 2999 (2012)
7. M.S. Howe, R.S. McGowan, The Journal of the Acoustical Society of America **133**(4), 2340 (2013)
8. P. Sidlof, , J. Horacek, V. Ridky, Computers and Fluids **80**, 290 (2013)
9. F. Alipour, C. Brücker, D. D Cook, A. Gömmel, M. Kaltenbacher, W. Mattheus, L. Mongeau, E. Nauman, R. Schwarze, I. Tokuda, S. Zörner, Current Bioinformatics **6**(3), 323 (2011)
10. R. Mittal, B.D. Erath, M.W. Plesniak, Annual Review of Fluid Mechanics **45**(1), 437 (2013)
11. M. Howe, R. McGowan, Journal of Sound and Vibration **332**(17), 3909 (2013)
12. W. Mattheus, C. Brücker, The Journal of the Acoustical Society of America **130**(6), EL373 (2011)
13. M. de Oliveira Rosa, J.C. Pereira, M. Grellet, A. Alwan, The Journal of the Acoustical Society of America **114**(5), 2893 (2003)
14. M. Mihaescu, S.M. Khosla, S. Murugappan, E.J. Gutmark, The Journal of the Acoustical Society of America **127**(1), 435 (2010)
15. X. Zheng, R. Mittal, S. Bielamowicz, Journal of the Acoustical Society of America **129(4)**(4), 2133 (2011)
16. X. Zheng, R. Mittal, Q. Xue, S. Beilamowicz, Journal of the Acoustical Society of America **130 (1)**, 404 (2011)
17. M. Triep, C. Brücker, Journal of the Acoustical Society of America **127**(2), 1537 (2010)
18. M. Triep, C. Brücker, W. Schröder, Experiments in Fluids **39**, 232 (2005)
19. M. Triep, C. Brücker, M. Stingl, M. Döllinger, Medical engineering and physics **33**(2), 210 (2011)
20. C. Kirmse, M.T. M, C. Brücker, M. Döllinger, M. Stingl, Logopedics, Phoniatrics, Vocology **35**, 45 (2010)
21. X. Pelorson, A. Hirschberg, R. van Hassel, A. Wijnands, Y. Auregan, Journal of the Acoustical Society of America **96**, 3416 (1994)
22. Y.J. Moon, J.H. Seo, S.R. Koh, Y.M. Bae, in *6th Asian Computational Fluid Dynamics Conference, Taiwan, Oct 24–27, 2005* (2005)
23. Y. Moon, J. Seo, Y. Bae, M. Roger, S. Becker, Computers and Fluids **39**(7), 1125 (2010)
24. Y.J. Moon, European Journal of Mechanics - B/Fluids **40**(0), 50 (2013)
25. H.G. Weller, G. Tabor, H. Jasak, C. Fureby, Computers in Physics **12**, 620 (1998)

26. B. van Leer, Journal of Computational Physics **32**(1), 101 (1979)
27. R. Issa, Journal of Computational Physics **62**(1), 40 (1986)
28. C. Rhie, L. Chow, AIAA J **21**, 1525 (1983)
29. R. Fletcher, Lecture Notes in Mathematics **506**, 73 (1976)
30. R. Schwarze, W. Mattheus, J. Klostermann, C. Brcker, Computers and Fluids **48**(1), 68 (2011)
31. M. Rothenberg, The Journal of the Acoustical Society of America **53**(6), 1632 (1973)
32. B. Doval, C. d'Alessandro, N. Henrich, Acta Acustica united with Acustica **92**(6), 1026 (2006)
33. J. Neubauer, Z. Zhang, R. Miraghaie, D. Berry, The Journal of the Acoustical Society of America **121**(2), 1102 (2007)
34. Y. Dubief, F. Delcayre, Jounal of Turbulence **1**, 1 (2000)